Eur. Phys. J. B **33**, 321–330 (2003)
DOI: 10.1140/epjb/e2003-00172-9

THE EUROPEAN PHYSICAL JOURNAL B

Magnetic properties of the cyclic spincluster Fe6:bicine

B. Pilawa[1,a], I. Keilhauer[1], G. Fischer[1], S. Knorr[2], J. Rahmer[2], and A. Grupp[2]

[1] Physikalisches Institut, Universität Karlsruhe (TH), Wolfgang Gaede Strasse 1, 76128 Karlsruhe, Germany
[2] 2. Physikalisches Institut, Universität Stuttgart, 70550 Stuttgart, Germany

Received 28 October 2002 / Received in final form 22 February 2003
Published online 20 June 2003

Abstract. The magnetic properties of the cyclic compound $[Fe_6(bicine)_6]$ $LiClO_4 \cdot 2MeOH$ are reported. The cluster $Fe_6(bicine)_6$ forms an antiferromagnetically coupled ring structure of Fe^{III} ions. The magnetic susceptibility is measured between 2 and 300 K and yields the exchange coupling of $J/k_B = -27.5 \pm 0.5$ K. The field dependence of the magnetic moment is studied at 3 and 6 K in magnetic fields up to 5 T. The zero-field splitting of the first excited spin states with $S = 2$ and 3 are determined by ESR at 94 GHz. The intra-molecular interactions of the Fe^{III} ions are analyzed and the on-site anisotropy of the Fe^{III} due to the ligand-configuration is determined to $d/k_B = -0.633 \pm 0.008$ K.

PACS. 33.35.+r Electron resonance and relaxation – 36.40.-c Atomic and molecular clusters – 75.20.-g Diamagnetism, paramagnetism, and superparamagnetism – 75.75.+a Magnetic properties of nanostructures

1 Introduction

Polynuclear metal complexes attract the interest for the variety of new magnetic properties, for the new physics involved and for the potential applications [1]. Molecular ring-systems present an interesting subgroup of magnetic molecular clusters, because their physical properties are expected to show features of an infinite chain, especially when the number of interacting spins increases [2]. The magnetic properties of such nanoscopic molecules result from the interplay of the dominating superexchange between the atomic spins, the dipolar coupling of the local moments, and the on-site spin anisotropy arising from the ligand configuration. Crystal lattices are often formed by the clusters and allow the measurement of isotropic and anisotropic magnetic properties of individual molecules on macroscopic samples since the clusters remain magnetically isolated. Information about the intra-molecular interactions can be obtained by measurements of the static magnetic susceptibility [3]. However, the magnetic susceptibility is not very sensitive to anisotropic interactions since it results from the thermal average of many occupied molecular eigenstates. It is possible to overcome this problem by measurements of the magnetic moment at low temperatures as a function of the applied magnetic field. The magnetization of the cyclic spin cluster increases step-like due to field induced level-crossings of the groundstate. The crossing of the levels can be sensitively detected by cantilever torque magnetometry and yields quasi spectroscopic information of the relative energy and the zero-field splitting of the excited spin states which cross the groundstate [4]. The method often relies on the assumption that the zero-field splitting of the spin states is determined by one parameter D_S, which is not necessarily true. Electron spin resonance (ESR) provides the direct approach to the zero-field splitting of spin-cluster compounds. However, usually the zero-field splitting of coupled systems of magnetic ions is large, so that the application of high frequencies and large magnetic fields is necessary in order to detect resonances. The groundstates of ferri/ferro-magnetically coupled clusters have been successfully studied by means of high-field/frequency ESR. Indeed the interpretation of the spectra simplifies considerably when the Zeeman energy becomes larger than the zero-field splitting [5]. In the case of the antiferromagnetically coupled spin clusters with a spin zero groundstate the thermally excited spin states have to be analyzed. This is complicated by the fact that the spectra of these spin states overlap [6]. In this paper we will show that detailed information about the electronic structure of the hexanuclear cyclic iron(III) cluster can be obtained by ESR even when the samples are contaminated by an unknown magnetic species. We report the magnetic properties of the spin cluster compound $[Fe_6(bicine)_6]$ $LiClO_4 \cdot 2MeOH$, which is abbreviated in the following as Fe6:bicine (bicine denotes N,N-Bis(2-hydroxyethyl)glycine). Fe6:bicine is studied by measurements of the static magnetic susceptibility and ESR at 94 GHz.

[a] e-mail: bernd@piobelix.physik.uni-karlsruhe.de

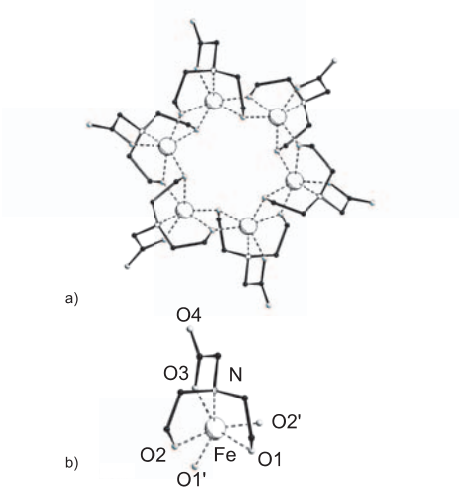

Fig. 1. a) View of the Fe6:bicine (SCHAKAL) along the $\bar{3}$ symmetry axis (H-atoms omitted). b) Detailed view of the coordination of the Fe atom. The black dots indicate C-atoms.

2 Experimental details and results

Fe6:bicine was synthesized by Geisselmann [7]. Figure 1 shows a projection of the Fe6:bicine cluster. The molecular point symmetry is $\bar{3}$.

The crystals form small green needles with a typical length $\lesssim 1$ mm and a diameter $\lesssim 0.3$ mm. The hexagonal unit cell contains two Fe6:bicine units as well as lithium, perchlorate, methanol and water molecules (space group, $P6_3/m$, a=13.8287 Å, c=18.0228 Å [7]. The Fe^{III} ions are bridged and magnetically coupled *via* two oxygen atoms located inside (atom O(1)) and outside (atom O(2)) of the iron ring. The molecular symmetry axis is parallel to the c direction of the crystal lattice. Some structural parameters of the Fe6:bicine cluster are compared in Table 1 with those of the related Fe_6tea_6 cluster (Fe6:tea, tea: triethanolaminate(3−)) which differs from the Fe6:bicine cluster only by the atom O(4) [6,8]. O(4) is replaced by two hydrogen atoms (compare Fig. 1). The magneto-structural properties of the two molecules are discussed and compared in Section 4. The static magnetic moment of oriented single crystals and polycrystalline samples was determined with a SQUID magnetometer (Quantum Design, Magnetic Property Measurement System) for magnetic field strengths up to 5.5 T in the temperature range 2 to 300 K. The experimental results are shown in Figure 2. For temperatures down to ≈ 40 K the static magnetic susceptibility varies as expected for the cyclic Fe6 cluster [3,6]. Below ≈ 40 K χ increases when the magnetic field is applied perpendicular to **c** and depends crucially on the strength of the applied magnetic field. When the magnetic field is applied parallel to **c** the susceptibility follows the expected temperature dependence down to ≈ 6 K. At lower temperatures there is a Curie-like increase of χ which also depends on the strength of the magnetic field. The inset in Figure 2 shows the field dependence of the magnetic moment for $\boldsymbol{B}\perp\mathbf{c}$ at 3 and 6 K. After a steep increase in the low field range the magnetic moment increases nearly linearly with B. The ESR measurements were carried out on single crystals with a Bruker ELEXSYS W-band spectrometer (94 GHz). The spectra were taken in the temperature range 6–40 K. The hysteresis of the superconducting coil of 30 G was corrected. The crystals (length $\lesssim$0.1 mm) were mounted with vacuum grease on a quartz rod so that the angle between **c** and $\boldsymbol{B}$ could be varied between 0° and 90°. The W-band spectra were taken in the field range between 0 and 5 T in angular steps of 15°. An overview of the spectra is given in Figure 3. The observed resonances are generally weak and at the limit of the experimental sensitivity. The orientation of the crystal can be deduced from the angular shift of the strong resonance in the range between 2 and 2.5 T. No ESR signals of the Fe6:bicine cluster could be observed at 9.5 GHz.

Table 1. Intra-molecular structural parameters of Fe6:bicine [7] and Fe6:tea [8]: Fe···Fe distance, inner/outer ◁(Fe-O(1)-Fe)/◁ (Fe-O(2)-Fe) bridging angle, and torsional angles (compare Fig. 1).

	Fe6:bicine	Fe6:tea
Fe . . . Fe	3.152 Å	3.201 Å
◁(Fe-O(1)-Fe)	103.99°	106.19°
◁ (Fe-O(2)-Fe)	104.17°	105.30°
◁ (O(3)-N-Fe-O(1))	159.3°	154.97°
◁(O(3)-N-Fe-O(1)')	−87.2°	−97.8°
◁(O(3)-N-Fe-O(2))	−104.3°	−108.0°
◁ (O(3)-N-Fe-O(2)')	87.9°	88.4°

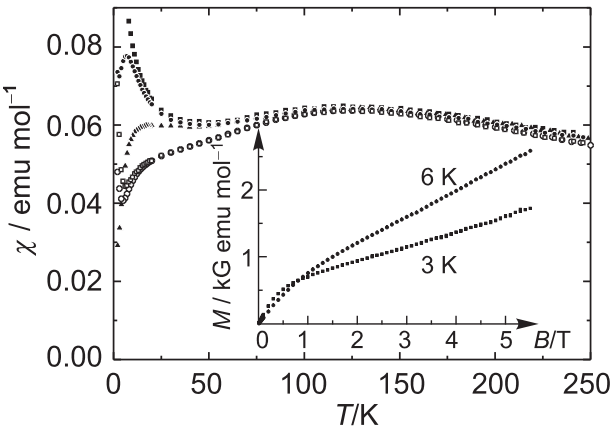

Fig. 2. Magnetic susceptibility of the Fe6:bicine cluster. The magnetic field is applied parallel (open symbols) and perpendicular to the hexagonal axis (full symbols). Squares: B = 0.1 T, circles: B = 1 T, triangles: B = 5 T. Inset: magnetic moment $\boldsymbol{B}\perp\mathbf{c}$.

3 Analysis of the experimental results

The static magnetic properties of the cyclic Fe6 clusters are essentially determined by the isotropic exchange interaction between the Fe^{III} ions $\mathcal{H}_{ex}$, the local anisotropy of the Fe^{III} ions caused by the ligand configuration

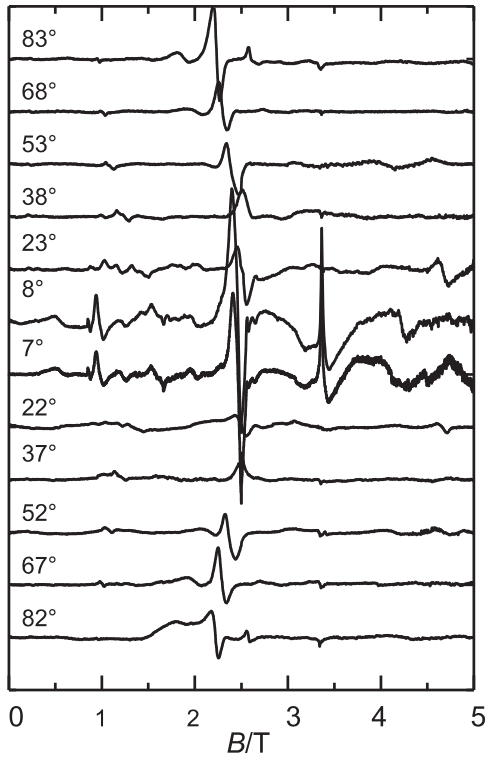

Fig. 3. ESR spectra at 94 GHz of a single crystal of Fe6:bicine. The numbers give the angle $\sphericalangle(\boldsymbol{B}, \mathbf{c})$.

$\mathcal{H}_{\rm ligand}$ and the intra-molecular dipolar interaction $\mathcal{H}_{\rm dipol}$. The Hamiltonian of the Fe6:bicine cluster has to transform like the total symmetric representation of the point group $\bar{3}$ which leads to the following expressions for the Hamiltonians

$$\mathcal{H}_{\rm ex} = -J \sum_{i=1}^{6} \boldsymbol{s}_i \boldsymbol{s}_{i+1}, \quad \boldsymbol{s}_1 = \boldsymbol{s}_7 \tag{1a}$$

$$\mathcal{H}_{\rm ligand} = d \sum_{i=1}^{6} \left((s_i^z)^2 - \frac{1}{3} (\boldsymbol{s}_i)^2 \right) \tag{1b}$$

and

$$\mathcal{H}_{\rm dipol} = (g\mu_{\rm B})^2 \frac{1}{2} \sum_{i \neq j}^{6} \frac{3}{2} (1 - 3\cos^2 \Theta_{ij}) \times \frac{1}{r_{ij}^3} \left(s_i^z s_j^z - \frac{1}{3} \boldsymbol{s}_i \boldsymbol{s}_j \right). \tag{1c}$$

Only the secular parts of $\mathcal{H}_{\rm ligand}$ and $\mathcal{H}_{\rm dipol}$ are invariant with respect to the $\bar{3}$ axis and contribute therefore to the Hamiltonian of the spin cluster. The angle Θ_{ij} equals 90° for all vectors $\boldsymbol{r}_{ij}$, since the Fe^{III} ions are arranged in a plane perpendicular to the quantization axis $\mathbf{z}(\mathbf{z}||\mathbf{c})$. The g-factor of the Fe^{III} ion is nearly isotropic. For the related system Fe6:tea it was shown by ESR at 9.5 GHz that the deviation from 2 is smaller than 10^{-3} [6]. Therefore $g = 2$ will be assumed in the following. The parameter d describing the on-site anisotropy of the Fe^{III} ion equals the $d_{zz}(i)$ component of the corresponding quadrupolar tensor. Hamiltonian equation (1b) yields therefore no information about the orientation of the local anisotropy axes of the Fe^{III} ions.

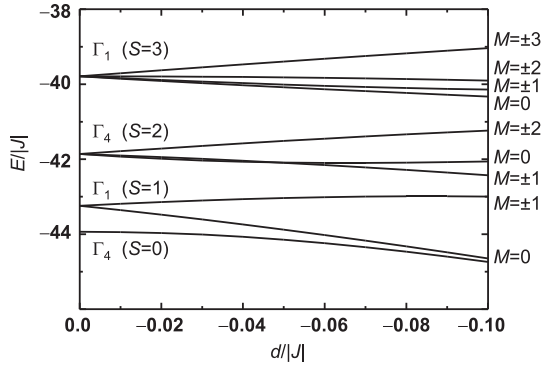

Fig. 4. The lowest energy levels of the Hamiltonian $\mathcal{H} = \mathcal{H}_{\rm ex} + \mathcal{H}_{\rm ligand}$.

The symmetry properties and energy spectrum of Hamiltonian equation (1) $\mathcal{H}_{\rm ex} + \mathcal{H}_{\rm ligand} + \mathcal{H}_{\rm dipol}$ was discussed several times *e.g.* [6,9]. Hamiltonian equation (1) is invariant under rotation of the coordinate system around $\mathbf{z}$ that is, Hamiltonian equation (1) commutes with $S^z = \sum s_i^z$ and the M quantum number of the total spin is a good quantum number. Hamiltonian equation (1) is also invariant under cyclic permutations of the indices so that the eigenstates of equation (1) transform according to the irreducible representations $\Gamma_t (t = 1, 2, ...6)$ of the group 6 [10]. The total spin states S are mixed by the anisotropic Hamiltonian equations (1b and c), so that S is not a good quantum number.

Exploiting these symmetries the Hamiltonian equation (1) reduces to matrices with the dimensions up to (depending on M) 721 and 724 for $t = 2, 3, 5, 6$ and 1, 4, respectively. The matrices can be calculated with the standard tensor-operator techniques [11]. Figure 4 shows the lowest energy levels of Hamiltonian $\mathcal{H} = \mathcal{H}_{\rm ex} + \mathcal{H}_{\rm ligand}$. The eigenstates are characterized by the symmetry label Γ_t, the S quantum number of the most important contribution to the eigenstate and the M quantum number. The degeneracy of the eigenstates of $\mathcal{H}_{\rm ex}$ is partially removed by $\mathcal{H}_{\rm ligand}$. Negative values of the parameter d for the on-site anisotropy of the Fe^{III} ion lead to the experimentally observed hard-axis anisotropy of the coupled spin system. Already small d values induce non-linear level shifts due to interactions between eigenstates of the same irreducible representation Γ_t and the same quantum number M. Therefore not only the parameter d but also the exchange constant J is important for the description of the zero-field splitting.

An external magnetic field which is not applied parallel to $\mathbf{z}$ breaks the S^z-symmetry of the Hamiltonian equation (1) and mixes the M quantum numbers. In order to analyze the experimental results only the properties of the lowest eigenstates are important and it is not necessary to

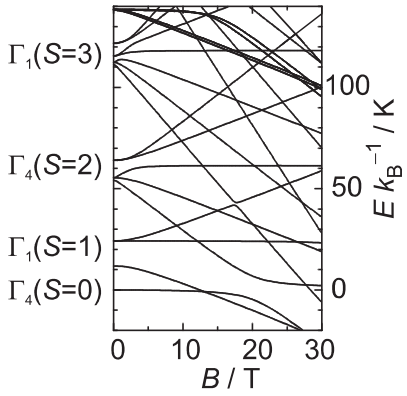

Fig. 5. Influence of a magnetic field applied perpendicular to the molecular symmetry axis on the lowest eigenstates of Hamiltonian equation (1).

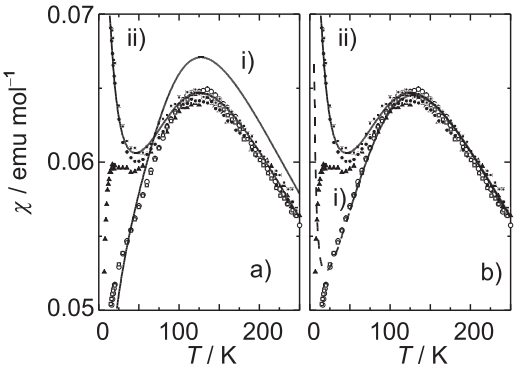

Fig. 6. Analysis of the static susceptibility. a: curve i) and ii) display the calculated susceptibility with and without the defect contribution, respectively. The anisotropy of the Fe6:bicine cluster is not included (details see text). b: the calculated susceptibility for parallel (curve i) and perpendicular field orientation (curve ii) when the anisotropy of the Fe6:bicine cluster is included (details see text).The symbols are the same as in Figure 2.

diagonalize the total matrix of the Hamiltonian

$$\mathcal{H} = \mathcal{H}_{\rm ex} + \mathcal{H}_{\rm ligand} + \mathcal{H}_{\rm dipol} + \mathcal{H}_{\rm Zee} \qquad (2)$$

$\mathcal{H}_{\rm Zee}$ denotes $\mathcal{H}_{\rm Zee}$=g$\mu_B \boldsymbol{B} \sum_{i=1}^{6} \boldsymbol{s}_i$. The Heisenberg Hamiltonian $\mathcal{H}_{\rm ex}$ can be solved by exploiting the symmetry properties of the total spin operator $\boldsymbol{S} = \sum_{i=1}^{6} \boldsymbol{s}_i$ [11]. The matrix of the non-Heisenberg Hamiltonian $\mathcal{H}_{\rm ligand} + \mathcal{H}_{\rm dipol} + \mathcal{H}_{\rm Zee}$ is calculated in a second step with those eigenfunctions of $\mathcal{H}_{\rm ex}$ which contribute to the thermally populated eigenstates at low temperatures when the magnetic anisotropy becomes important. In the following calculations all eigenstates of $\mathcal{H}_{\rm ex}$ up to $9|J|$ above the groundstate $\Gamma_4(S = 0)$ are included [12]. Figure 5 shows the influence of the Zeeman Hamiltonian $\mathcal{H}_{\rm Zee}$ with $\boldsymbol{B}\perp\mathbf{c}$. Figure 5 is calculated with the parameters of the Fe6:bicine system $g = 2$, $J/k_B = -27.5$ K and $d/k_B = -0.633$ K (see below) up to a field strength of 30 T in order to demonstrate the level crossing of states with different Γ_t labels and the anticrossing due to the Zeeman effect of states with the same Γ_t labels. The calculation includes the influence of the dipolar interaction (Hamiltonian Eq. (1c)). Since the anisotropic Hamiltonian equation (1b, c) induces a mixing of the S states, an interaction can be expected between eigenstates which belong to the same irreducible representation Γ_t, even when they are characterized by different S numbers. This is clearly visible for the interaction between the $\Gamma_4(S = 0), M = 0$ and the $\Gamma_4(S = 2), M = 0$ states for $B \gtrsim 20$ T (the eigenstates of Hamiltonian Eq. (2) are denoted by their symmetry labels and the M quantum number at $B = 0$). Since the ESR experiments are carried out in a magnetic field up to 5 T, the influence of the interaction between eigenstates $\Gamma_t(S)$ with different S numbers is small, though not completely negligible (see below).

3.1 Susceptibility

The magnetic susceptibility of Figure 2 shows that the Fe6:bicine crystals not only contain the molecular ring system but in addition some defect species which lead to an extremely anisotropic and field-dependent low-temperature susceptibility. All the synthetic attempts failed to get rid of these defect species [13]. Therefore the data shown in Figure 2 have to be used in order to estimate at least the parameters J and d of the Fe6:bicine cluster.

The magnetic moment of a molecular system is given by $\boldsymbol{m} = g\mu_B \langle \sum_i \boldsymbol{s}_i \rangle$ and can be calculated with the eigenstates of the Hamiltonian equation (1b, 2). The static magnetic susceptibility is defined by the quotient $\chi_{\rm Fe6:bicine} = \frac{M}{H}$ of the magnetization $M = Nm$ along the direction of the applied magnetic field $\boldsymbol{H}$ (N denotes the number of the magnetic molecules). Curve i) in Figure 6a shows the susceptibility when only the eigenfunctions of $\mathcal{H}$=$\mathcal{H}_{\rm ex}$ +$\mathcal{H}_{\rm Zee}$ are used to calculate $\langle \sum_i \boldsymbol{s}_i \rangle$. The fit of the maximum yields $J/k_{\rm B}$=-25.5 ± 0.5 K but the high temperature slope of χ indicates a stronger antiferromagnetic coupling of the Fe^{III} ions.

In a simple approach it can be assumed that a certain fraction c of the Fe6:bicine clusters are decomposed into six independent Fe^{III} complexes so that the susceptibility can be written as $\chi = (1-c)\chi_{\rm Fe6:bicine} + 6 \cdot c\chi_{S=5/2} + \chi_0$, with the susceptibility $\chi_{S=5/2}$ of a Fe^{III} ion and the temperature independent diamagnetic core susceptibility $\chi_0 (\approx -10^{-4}$ emu/mol). Curve ii) in Figure 6a shows the fit of the perpendicular susceptibility with $B = 0.1$ T. The susceptibility of the Fe6:bicine cluster is again determined only by the isotropic part $\chi_{\rm ex}$ of Hamiltonian equation (2) and the parameters are $J/k_B = -27.5 \pm 0.5$ K and $c = 1.75\%$. This result shows that only a comparatively small fraction of the molecular rings are damaged. The susceptibility of the defect shifts the temperature of the maximum at 127 K and can therefore not be neglected even at high temperatures.

The simple approach fails to describe the perpendicular susceptibility at $B = 5$ T and the measurements of the

parallel susceptibility. Obviously the defect species are not only simple Fe^{III} complexes [14]. However the anisotropy and field dependence of the defect susceptibility fades away with increasing temperature so that the difference between $\chi_{||}$ and $\chi_{\perp}$ above $T \approx 50$ K can be used to estimate the anisotropy of the Fe_6:bicine cluster.

The expectation value $\langle \sum_i \boldsymbol{s}_i \rangle$ has to be calculated with the eigenfunctions of the Hamiltonian $\mathcal{H} = \mathcal{H}_{\rm ex} + \mathcal{H}_{\rm ligand} + \mathcal{H}_{\rm dipol} + \mathcal{H}_{\rm Zee}$. For the fit of the susceptibility it is sufficient to diagonalize the matrix of $\mathcal{H}$ within the basis of the eigenstates of $\mathcal{H}_{\rm ex}$ up to an energy of $E_{\rm Cut} = 9|J|$ above the groundstate and to approximated the eigenstates at higher energies by the Hamiltonian $\mathcal{H} = \mathcal{H}_{\rm ex} + \mathcal{H}_{\rm Zee}$ [12]. The accuracy of this approach depends on the strength of the on-site anisotropy d and the temperature. The error can be estimated by an extrapolation $1/n \to 0$ of $\chi(n)$ calculated with $E_{\rm Cut} = n|J|, n = 3, 4, ..., 9$. With the parameters given below the maximal error of about 3% is found in the temperature range around $T \approx 40$ K. The curves i) and ii) in Figure 6b are calculated with the parameters $J/k_B = -27.2$ K, $c = 1.3\%$, $d/k_B = -0.56$ K and $B_{||} = B_{\perp} = 1$ T. The curves ii) in Figure 6a and b are nearly identical. The value of d is not too far from the ESR result $d/k_B = -0.633$ K (see below).

3.2 ESR

It will be shown in the following that the ESR spectra at 94 GHz originate from the $\Gamma_4(S = 2)$ and $\Gamma_1(S = 3)$ eigenstates of the Fe6:bicine cluster.

The description of the zero-field splitting of the $\Gamma_4(S = 2)$ and $\Gamma_1(S = 3)$ eigenstates is possible in terms of an effective spin Hamiltonian

$$\mathcal{H}_{S=2} = B_2^{(S=2)}(S_z)^2 + B_4^{(S=2)}(S_z)^4 \tag{3a}$$

and

$$\mathcal{H}_{S=3} = B_2^{(S=3)}(S_z)^2 + B_4^{(S=3)}(S_z)^4 + B_6^{(S=3)}(S_z)^6, \tag{3b}$$

within the spin space $S = 2$ and 3, respectively. Due to the axial symmetry of Hamiltonian equation (1) there are no transversal components of the effective spin Hamiltonian so that there exist a simple linear relation between the zero-field splitting $\Delta_M^{(S)} = E_{\pm M}^{(S)} - E_{M=0}^{(S)}$ and the parameters $B_q^{(S)}$ of the spin Hamiltonian

$$B_2^{(S=2)} = \left(16\Delta_1^{(S=2)} - \Delta_2^{(S=2)}\right)/12, \tag{4a}$$

$$B_4^{(S=2)} = \left(\Delta_2^{(S=2)} - 4\Delta_1^{(S=2)}\right)/12 \tag{4b}$$

for $S = 2$ and

$$B_2^{(S=3)} = \left(540\Delta_1^{(S=3)} - 54\Delta_2^{(S=3)} + 4\Delta_3^{(S=3)}\right)/360, \tag{5a}$$

$$B_4^{(S=3)} = \left(-39\Delta_1^{(S=3)} + 12\Delta_2^{(S=3)} - \Delta_3^{(S=3)}\right)/72, \tag{5b}$$

$$B_6^{(S=3)} = \left(15\Delta_1^{(S=3)} - 6\Delta_2^{(S=3)} + \Delta_3^{(S=3)}\right)/360 \tag{5c}$$

for $S = 3$.

According to Figure 4 the zero-field splittings depend on the parameter d of the on-site anisotropy of the Fe^{III} ions so that the experimentally determined values of $\Delta_M^{(S)}$ open a way to test the Hamiltonian of the Fe6:bicine cluster.

As mentioned above the ESR experiments were carried out in magnetic fields up to 5 T. In this field range, the results of Figure 5 show that the Zeeman effect of the eigenstates $\Gamma_4(S = 2)$ and $\Gamma_1(S = 3)$ can be modeled in a first order perturbation approach by a Zeeman-Hamiltonian $\mathcal{H}_{\rm Zeeman}^{(S)} = g\mu_B \boldsymbol{S}\boldsymbol{B}$ acting in the spin space $S = 2$ and 3, respectively. The absorption spectrum can be simulated by means of the eigenfunctions and eigenvalues of the spin Hamiltonians $\mathcal{H}_S + \mathcal{H}_{\rm Zeeman}^{(S)}$. Throughout the calculations the transition probability is approximated by a Lorentzian shaped function (the width of the Lorentz function was $\Delta B_{1/2} = 60$ mT) multiplied by the transition matrix element and the thermal occupation difference of the corresponding energy levels. Thereby the expected shape and intensity of the resonances can be visualized although it is not possible to account for the observed linewidth variations.

The description of the Zeeman effect by a first order approach has to be checked before it can be used for the investigation of the experimental spectra. For $\boldsymbol{B}||\mathbf{c}$, this approach is strictly correct, since there is no level mixing due to $\mathcal{H}_{\rm Zee}$. When the magnetic field is not parallel to $\mathbf{c}$, the interaction between the $\Gamma_t(S)$ eigenstates can even lead to level anticrossing as is shown in Figure 5. In order to estimate the influence of this interaction the Zeeman effect was calculated with Hamiltonian equation (2) ($J = -28$ K, $d = -0.6$ K) and the corresponding spin Hamiltonian equation (3) with $\boldsymbol{B} \perp \mathbf{c}$ for the $\Gamma_4(S = 2)$ and $\Gamma_1(S = 3)$ eigenstates, *i.e.* the parameters of Hamiltonian equation (3) are adjusted so that the zero-field splitting $\Delta_M^{(S)}$ determined by Hamiltonian equations (2) and (3) are the same. At 5 T the difference between the Zeeman splittings calculated with Hamiltonian equations (2) and (3) is smaller than $\Delta E/\mu_B \lesssim 153$ mT ($\lesssim 1.11\%$ of the Zeeman splitting between neighboring energy levels) and $\Delta E/\mu_B \lesssim 21$ mT ($\lesssim 0.21\%$) for the $\Gamma_4(S = 2)$ and $\Gamma_1(S = 3)$ eigenstates, respectively. Although the effect is small, it can be expected that the ESR resonances may be shifted in the range of several 10 mT due to the field induced interaction between the $\Gamma_t(S)$ eigenstates. The effective Zeeman operator $\mathcal{H}_{\rm Zeeman}^{(S)}$ cannot account for this effect. The analysis of the spectra by means of Hamiltonian equation (3) should therefore be applied to resonances in low magnetic fields ($\lesssim 2$T) and/or to spectra with small angles between $\boldsymbol{B}$ and $\mathbf{c}$.

In an ideal situation the spectra obtained for $\boldsymbol{B}||\mathbf{c}$ display more or less directly the zero-field splittings $\Delta_M^{(S)}$ (compare Ref. [6b]). In the case of Fe6:bicine the spectra lines are weak and noisy, so that the information has to be obtained by a combined analysis of the spectra for various field orientations. The analysis is based on the spectra $\sphericalangle(B, c) = 83°/82°$ (Fig. 7), $\sphericalangle(B, c) = 7°/8°$ (Fig. 8), $\sphericalangle(B, c) = 22°/23°$ (Fig. 9) and $\sphericalangle(B, c) = 52°/53°$

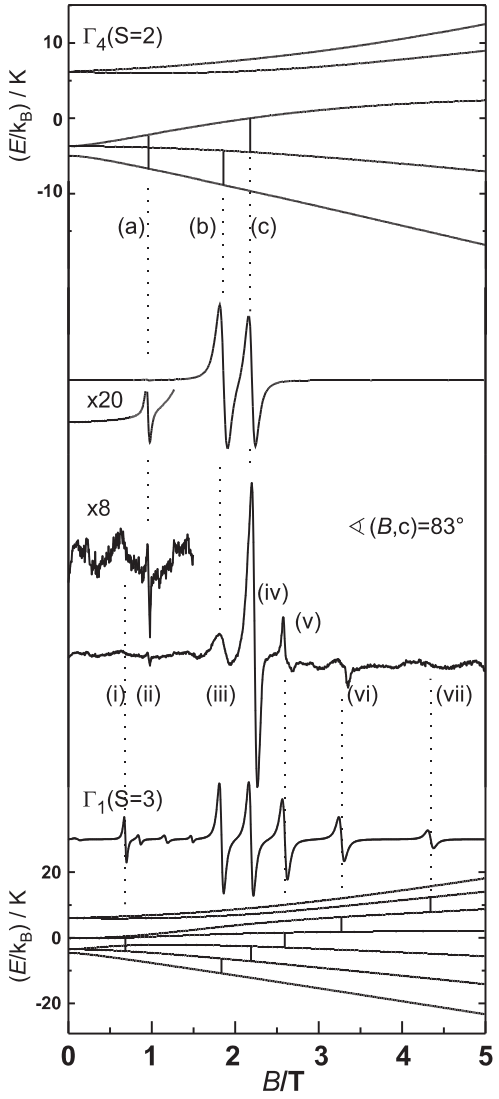

Fig. 7. Analysis of the spectrum $\sphericalangle(B,c) = 83°$. Upper part: Zeeman splitting of the $\Gamma_4(S = 2)$ eigenstates and the simulated ESR spectrum. Lower part: Zeeman splitting of the $\Gamma_1(S = 3)$ eigenstates and the simulated ESR spectrum. Central part: measured ESR spectrum at $T = 20$ K.

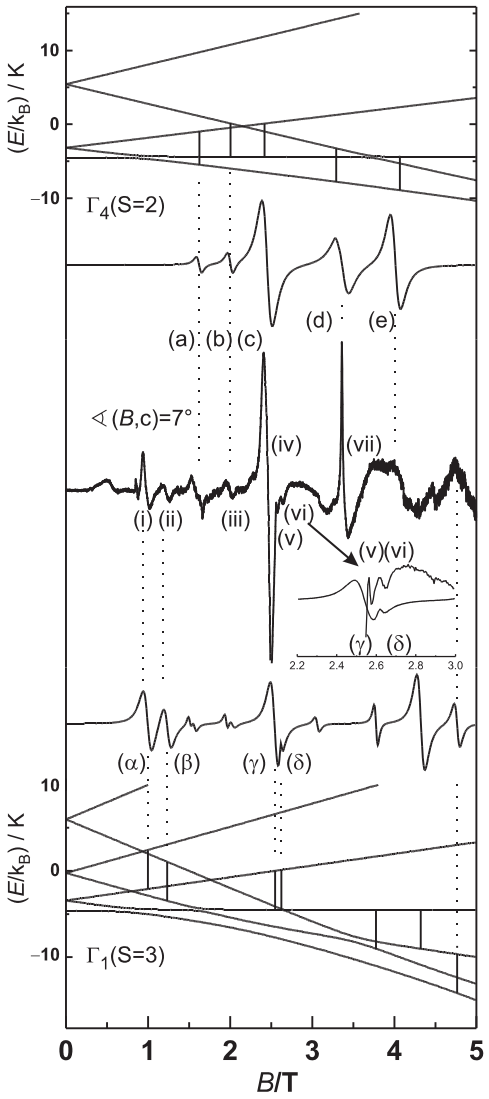

Fig. 8. Analysis of the spectrum $\sphericalangle(B,c) = 7°$. Upper part: Zeeman splitting of the $\Gamma_4(S = 2)$ eigenstates and the simulated ESR spectrum. Lower part: Zeeman splitting of the $\Gamma_1(S = 3)$ eigenstates and the simulated ESR spectrum. Central part: measured ESR spectrum at $T = 20$ K. Inset: details in the wing of line (iv).

(Fig. 10). The detailed comparison between the experimentally determined and simulated spectra is only shown for one orientation of the magnetic field, respectively. The remaining spectra provide no additional information. The experimentally determined spectra lines are denoted by small Latin letters (i), (ii), ..., the simulated lines of the $\Gamma_4(S = 2)$ eigenstates by small Latin letters (a), (b)... and the lines of the $\Gamma_1(S = 3)$ eigenstates by small Greek letters (α), (β)... .

3.2.1 The zero-field splitting of the $\Gamma_4(S = 2)$ eigenstates

The analysis of the $\Gamma_4(S = 2)$ eigenstates starts with the spectrum $\sphericalangle(\mathbf{c}, \boldsymbol{B}) = 83°$ shown in Figure 7. The resonance (a) is forbidden when the field is applied perpendicular to $\mathbf{c}$. Due to the deviation from the perpendicular field orientation it can be observed and it is assumed that the resonance (ii) belongs to the $\Gamma_4(S = 2)$ eigenstates. Since resonance (a) is sharp and does not depend strongly on the crystal orientation it fixes accurately the energy difference $\Delta_{M=1}^{(S=2)}$.

Once the values of $\Delta_{M=1}^{(S=2)}$ is fixed the resonances (b) and (c) are essentially determined although there is a small influence of the excited $M = \pm 2$ states. The spectrum $\sphericalangle(\mathbf{c}, \boldsymbol{B}) = 7°$ (Fig. 8) confirms the $\Delta_{M=1}^{(S=2)}$ value. The resonances (c) and (e) are determined by $\Delta_{M=1}^{(S=2)}$. The weak transition (b) in the spectrum $\sphericalangle(\mathbf{c}, \boldsymbol{B}) = 7°$ is assigned to line (iii) which determines the energy difference $\Delta_{M=2}^{(S=2)}$.

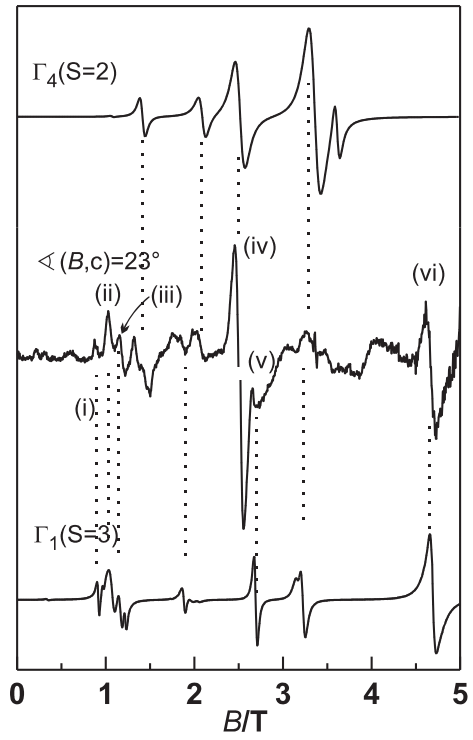

Fig. 9. Analysis of the spectrum $\sphericalangle(B,c) = 23°$. Upper part: simulated ESR spectrum of the $\Gamma_4(S = 2)$ eigenstates. Lower part: simulated ESR spectrum of the $\Gamma_1(S = 3)$ eigenstates. Central part: measured ESR spectrum at $T = 20$ K.

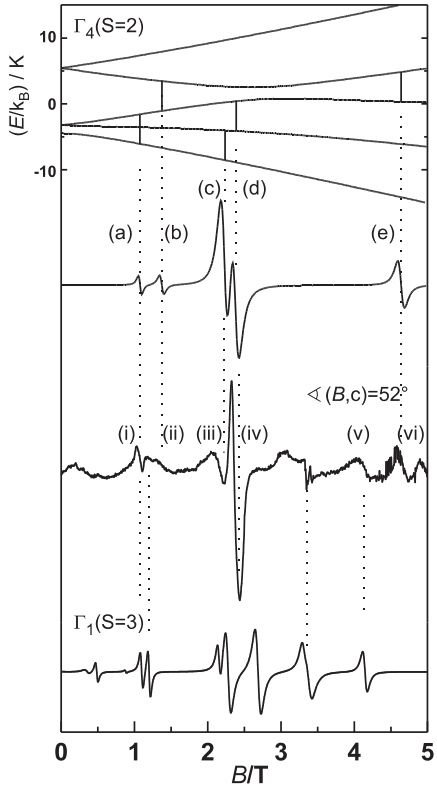

Fig. 10. Analysis of the spectrum $\sphericalangle(B,c) = 52°$. Upper part: Zeeman splitting of the $\Gamma_4(S = 2)$ eigenstates and simulated ESR spectrum. Lower part: simulated ESR spectrum of the $\Gamma_1(S = 3)$ eigenstates. Central part: measured ESR spectrum at $T = 20$ K.

Table 2. The experimentally determined zero-field splitting $\Delta_M^{(S)}$ and the resulting anisotropy parameter d of the Fe^{III} ions (compare Fig. 11). *) the experimentally determined splitting $\Delta_{M=1}^{(S=3)}$ is always larger than the calculated value (compare Fig. 11).

	experiment	d (without $\mathcal{H}_{\text{dipol}}$)	d (with $\mathcal{H}_{\text{dipol}}$)
		$\Gamma_4(S = 2)$	
$\Delta_{M=1}^{(S=2)}/k_B$	1.317±0.013 K	-*)	−0.631±0.028
$\Delta_{M=2}^{(S=2)}/k_B$	9.924±0.034 K	−0.747±0.003	−0.641±0.004
		$\Gamma_1(S = 3)$	
$\Delta_{M=1}^{(S=3)}/k_B$	1.147 ± 0.034 K	−0.782 ± 0.025	−0.660±0.025
$\Delta_{M=2}^{(S=3)} - \Delta_{M=1}^{(S=3)}/k_B$	3.296 ± 0.017 K	−0.748±0.005	−0.629±0.004
$\Delta_{M=3}^{(S=3)} - \Delta_{M=2}^{(S=3)}/k_B$	6.203±0.020 K	−0.745±0.002	−0.624±0.002

The correctness of $\Delta_{M=2}^{(S=2)}$ is confirmed by the spectra with $\sphericalangle(\mathbf{c}, \boldsymbol{B}) = 23°$ (Fig. 9) and $\sphericalangle(\mathbf{c}, \boldsymbol{B}) = 52°$ (Fig. 10).

The transition (d) and line (vii) in the spectrum $\sphericalangle(\mathbf{c}, \boldsymbol{B}) = 7°$ coincide accidentally. The position of line (vii) does not depend on the crystal orientation, whereas transition (d) is strongly shifted. Moreover line (vii) is the only one which can be observed even at the lowest measured temperature of 6 K. It is very likely that line (vii) does not originate from the Fe6:bicine cluster.

The zero-field splitting of the $\Gamma_4(S = 2)$ eigenstates $\Delta_{M=1}^{(S=2)}$ and $\Delta_{M=2}^{(S=2)}$ are given in Table 2. The parameters of the effective spin Hamiltonian equation (3a) are $B_2^{(S=2)}/k_B = 0.93 \pm 0.02$ K and $B_4^{(S=2)}/k_B = 0.388 \pm 0.007$ K. The error results from the uncertainty of the orientation (±1°) and the limitations of the first order calculation of the Zeeman effect, which permits only the prediction of a resonance field strength within a range of up to ±50 mT. The average difference between the observed and

calculated resonance field strengths is ±35 mT (for details of the fits see [15]). The large value of $B_4^{(S=2)}$ confirms that the fourth order contribution to the effective spin Hamiltonian cannot be neglected. The parameters of the Fe6:tea cluster are in the same range $B_2^{(S=2)}/k_B = 1.23$ K and $B_4^{(S=2)}/k_B = 0.31$ [6b].

3.2.2 The zero-field splitting of the $\Gamma_4(S = 3)$ eigenstates

The three energy differences $\Delta_{M=1}^{(S=3)}$, $\Delta_{M=2}^{(S=3)}$, and $\Delta_{M=3}^{(S=3)}$ have to be fixed for the $\Gamma_1(S = 3)$ eigenstates. The energy difference $\Delta_{M=3}^{(S=3)} - \Delta_{M=2}^{(S=3)} = E_{M=\pm3}^{(S=3)} - E_{M=\pm2}^{(S=3)}$ is well determined by the observed resonances. The transition (β) is attributed to resonance (ii) in the $\sphericalangle(\mathbf{c}, \boldsymbol{B}) = 7°$ spectrum (Fig. 8). As a consequence of this assignment the lines (iii), (v) and (vi) in the spectrum with $\sphericalangle(\mathbf{c}, \boldsymbol{B}) = 23°$ (Fig. 9) can be attributed to the $\Gamma_1(S = 3)$ eigenstates. The simulation of these resonances depends sensitively on the energy difference $E_{M=\pm3}^{(S=3)} - E_{M=\pm2}^{(S=3)}$ and confirms the assignment.

The energy difference $\Delta_{M=2}^{(S=3)} - \Delta_{M=1}^{(S=3)} = E_{M=\pm2}^{(S=3)} - E_{M=\pm1}^{(S=3)}$ can be estimated from the spectrum with $\sphericalangle(\mathbf{c}, \boldsymbol{B}) = 83°$ (Fig. 7, lines i, v, vi). However the resonance positions depend not very sensitively on $E_{M=\pm2}^{S=3} - E_{M=\pm1}^{(S=3)}$. In the spectrum $\sphericalangle(\mathbf{c}, \boldsymbol{B}) = 23°$ (Fig. 9) the lines (i) and (ii) can be attributed to the $\Gamma_1(S = 3)$ eigenstates. The resonance positions of these lines depend sensitively on $E_{M=\pm2}^{(S=3)} - E_{M=\pm1}^{(S=3)}$ and allow an accurate determination of the zero-field splitting $\left(E_{M=\pm2}^{(S=3)} - E_{M=\pm1}^{(S=3)}\right)/k_B = 3.296 \pm 0.017$ K. The qualitative comparison with the spectrum $\sphericalangle(\mathbf{c}, \boldsymbol{B}) = 52°$ in Figure 10 confirms the value of the energy difference $E_{M=\pm2}^{(S=3)} - E_{M=\pm1}^{(S=3)}$.

In the spectrum with $\sphericalangle(\mathbf{c}, \boldsymbol{B}) = 7°$ the line (i) is very close to the transition (α) which fixes $E_{M=\pm2}^{(S=3)} - E_{M=\pm1}^{(S=3)}$. The fit of this line results in a slightly smaller zero-field splitting of $\left(E_{M=\pm2}^{(S=3)} - E_{M=\pm1}^{(S=3)}\right)/k_B = 3.232 \pm 0.014$ K, which however cannot describe the spectra with $\sphericalangle(\mathbf{c}, \boldsymbol{B}) = 23°$ and $\sphericalangle(\mathbf{c}, \boldsymbol{B}) = 52°$. Line (i) probably does not originate from the $\Gamma_1(S = 3)$ eigenstates.

The energy difference $\Delta_{M=1}^{(S=3)} = E_{M=\pm1}^{(S=3)} - E_{M=0}^{(S=3)}$ cannot be determined easily since the corresponding transitions overlap with lines of the $\Gamma_4(S = 2)$ spectrum (see Figs. 7 and 8). The small resonance (v) in the wing of the strong line (iv) in the $\sphericalangle(\mathbf{c}, \boldsymbol{B}) = 7°$ spectrum might be caused by transition (γ) which depends on $\Delta_{M=1}^{(S=3)}$. As a consequence of this assignment there is a weak transition (δ) which results from the forbidden $M = -3 \leftrightarrow M = +1$ transition. This transition becomes visible due to mixing of the $M = 0, -3$ states in the neighborhood of the anticrossing of these states (see Fig. 7, the anticrossing effect is however too small to be resolved in Fig. 8). Transition (δ) is attributed to the weak line (vi) which confirms that the energy differences $\Delta_{M=3}^{(S=3)} - \Delta_{M=2}^{(S=3)} = E_{M=\pm3}^{(S=3)} - E_{M=\pm2}^{(S=3)}, \Delta_{M=2}^{(S=3)} - \Delta_{M=1}^{(S=3)} = E_{M=\pm2}^{(S=3)} - E_{M=\pm1}^{(S=3)}$ and $\Delta_{M=1}^{(S=3)} = E_{M=\pm1}^{(S=3)} - E_{M=0}^{(S=3)}$ are correctly determined (see inset of Fig. 8). The exact value of $\Delta_{M=1}^{(S=3)}$ might be distorted due to the neighborhood of line (v) and the strong line (iv).

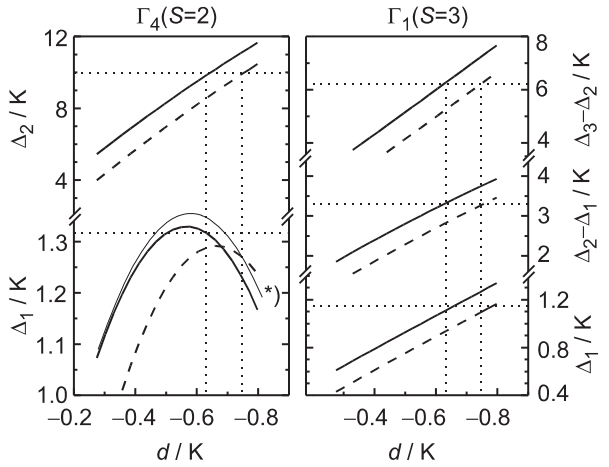

Fig. 11. Relation between the zero-field splitting and the anisotropic interactions of the Fe6:bicine cluster. Broken line: zero-field splitting calculated with $\mathcal{H} = \mathcal{H}_{\rm ex} + \mathcal{H}_{\rm ligand}$. Solid line: zero-field splitting calculated with $\mathcal{H} = \mathcal{H}_{\rm ex} + \mathcal{H}_{\rm ligand} + \mathcal{H}_{\rm dipol}$ ($J/k_B = -27.5$ K). Marked curve (∗) calculated with $\mathcal{H} = \mathcal{H}_{\rm ex} + \mathcal{H}_{\rm ligand} + \mathcal{H}_{\rm dipol}$ and $J/k_B = -28$ K.

The zero-field splitting of the $\Gamma_1(S = 3)$ eigenstates $\Delta_{M=1}^{(S=3)}, \Delta_{M=2}^{(S=3)} - \Delta_{M=1}^{(S=3)}$ and $\Delta_{M=3}^{(S=3)} - \Delta_{M=2}^{(S=3)}$ are given in Table 2. The parameters of the effective spin Hamiltonian equation (3b) become $B_2^{(S=3)}/k_B = 1.295 \pm 0.054$ K, $B_4^{(S=3)}/k_B = -0.158 \pm 0.022$ K and $B_6^{(S=3)}/k_B = -0.010 \pm 0.002$ K. Although the parameters $B_4^{(S=3)}$ and $B_6^{(S=3)}$ are small compared with $B_2^{(S=3)}$, they are considerably larger than those of the Fe6:tea cluster ($B_2^{(S=3)}/k_B = 1.08$ K, $B_4^{(S=3)}/k_B = -0.28$ mK and $B_6^{(S=3)}/k_B = 0.1348$ mK [6b]).

4 Discussion

The zero-field splittings $\Delta_M^{(S)}$ of the $\Gamma_t(S)$ eigenstates are determined by the microscopic spin Hamiltonian equation (1) of the Fe6:bicine cluster (compare Fig. 4). Figure 11 shows the variation of the zero-field splittings $\Delta_M^{(S)}$ as a function of the component $d = d_{zz}(i)$ of the quadrupolar tensor describing the on-site anisotropy of the Fe^{III} ion for the $\Gamma_4(S = 2)$ and $\Gamma_1(S = 3)$ eigenstates. The calculation is carried out with and without the dipolar interaction. The influence of the isotropic exchange interaction on the zero-field splitting is (aside from $\Delta_{M=1}^{(S=2)}$ of $\Gamma_4(S = 2)$) negligible when J is varied in the range between -27 and -28 K. Figure 11 is calculated with $J/k_B = -27.5$ K. The nonlinear behavior of the splitting $\Delta_{M=1}^{(S=2)}$ of $\Gamma_4(S = 2)$ is caused by the interaction between $\Gamma_4(S = 2)$ and the

groundstate $\Gamma_4(S=0)$ (compare Fig. 4). Due to this interaction $\Delta_{M=1}^{(S=2)}$ of $\Gamma_4(S=2)$ also depends on J. As an example, the marked line in Figure 11 is calculated with $J/k_B = -28$ K (and the dipolar interaction included).

d can be determined by means of the experimental zero-field splittings $\Delta_{M=1}^{(S=2)}$ (dotted lines in Fig. 11). The resulting d-values are given in Table 2. For the $\Delta_{M=1}^{(S=2 \text{ or } 3)}$ splitting the experimental error results in a particularly large error of d due to the nonlinear behavior ($\Gamma_4(S=2)$) and the small slope ($\Gamma_1(S=3)$) of the $\Delta_{M=1}^{(S)}(d)$ curves. For $\Delta_{M=1}^{(S=2)}$ of ($\Gamma_4(S=2)$) the error of d has to be enhanced due to the uncertainty of J.

When the dipolar interaction is neglected $\Delta_{M=2}^{(S=2)}$,$\Delta_{M=2}^{(S=3)} - \Delta_{M=1}^{(S=3)}$ and $\Delta_{M=3}^{(S=3)} - \Delta_{M=2}^{(S=3)}$ yield the consistent value $d/k_B = -0.747 \pm 0.002$ K. When the dipolar interaction is included in the description of the $\Gamma_4(S=2)$ eigenstates, $\Delta_{M=2}^{(S=2)}$ yields $d/k_B = -0.641 \pm 0.004$ K and the d determined by $\Delta_{M=1}^{(S=2)}$ is compatible with this value. As is shown in Figure 11 this result confirms the exchange constant of $J/k_B = -27.5$ K. The energy differences $\Delta_{M=2}^{(S=3)} - \Delta_{M=1}^{(S=3)}$ and $\Delta_{M=3}^{(S=3)} - \Delta_{M=2}^{(S=3)}$ of the $\Gamma_1(S=3)$ eigenstates demand the somewhat larger value $d/k_B = -0.625 \pm 0.004$ K. d determined by $\Delta_{M=1}^{(S=3)}$ is not compatible with this value. The estimation of the experimental error of $\Delta_{M=1}^{(S=3)}$ is probably too small (compare Sect. 3.2.2). The small difference between the d values of the $\Gamma_4(S=2)$ and the $\Gamma_1(S=3)$ eigenstates might indicate that aside from the quadrupolar on-site anisotropy of the Fe^{III} ion and the dipolar interactions there are additional anisotropic interactions (anisotropic exchange or higher order components of the on-site anisotropy) which contribute to the zero-field splitting. Neglecting these additional anisotropic interactions, the average d value of the Fe^{III} ions is $d/k_B = -0.633 \pm 0.008$ K.

The values J and d of the Fe6:bicine ring can be used to predict the spectra of other spin states. Especially for the first excited $\Gamma_1(S=1)$ eigenstates a zero-field splitting of $\Delta_{M=1}^{(S=1)}/k_B = 12.32 \pm 0.14$K can be expected according to the above results. The $M = 0 \leftrightarrow -1$ transition with $\boldsymbol{B}||\mathbf{c}$ should be observed at a field strengths of 9.166 ± 0.110 T, which is well above the maximal magnetic field of our spectrometer ($B < 6$ T). When the magnetic field is not applied parallel $\mathbf{c}$, the forbidden transition $M = +1 \leftrightarrow -1$ is of low absorption intensity and the corresponding field strength depends critically on the orientation of the crystal within the magnetic field. With the available spectra the $M = +1 \leftrightarrow -1$ transition cannot be traced. It can be definitively concluded that the strong resonances (i) and (vii) in the spectra $\sphericalangle(\mathbf{c}, \boldsymbol{B}) = 7°$ and 8° (see Fig. 8) cannot be assigned to the $\Gamma_1(S=1)$ eigenstates. Probably these resonances originate from the unknown defect species observed by the susceptibility measurements. This is confirmed by the fact that both these resonances and the defect susceptibility are very anisotropic (the lines (i) and (vii) can only be observed, when $\boldsymbol{B}$ is applied approximately parallel to $\mathbf{c}$).

The parameters of the related Fe6:tea cluster are $J/k_B = -31.5$ K and $d/k_B = -0.603 \pm 0.008$ K. The local anisotropy and the dipolar interaction are weaker in the Fe6:tea cluster than in the Fe6:bicine cluster, whereas the exchange coupling of the Fe^{III} is stronger for Fe6:tea than for Fe6:bicine. Consequently, the interaction between the Γ_t eigenstates due to the anisotropic interactions is more important for the Fe6:bicine system than for the Fe6:tea system which leads to the experimentally observed enhancement of the higher order terms $B_q^{(S)}$ in the effective spin Hamiltonian equation (3).

The exchange constant J varies for the various Fe6:tea clusters with the $\sphericalangle$(Fe-O(1)-Fe) angle α_1 according to $J[K] = -2.91\alpha_1[°] + 276$ [4b]. The formula predicts for the Fe6:bicine cluster with $\alpha_1 = 104° J/k_B = -26.6$ K and with $\alpha_1 = 106.2°$ for the Fe6:tea cluster $J/k_B = -33.0$ K which is very close to the experimental values. On the other hand the on-site anisotropy d can be correlated with the torsional angle $\varphi = \sphericalangle$(O(3)-N-Fe-O(1)′) which is the most sensitive parameter describing the coordination environment of the Fe^{III} ion [4b]. Comparing Table 1 the rule that $|d|$ decreases when $|\varphi|$ increases is indeed confirmed by the comparison between the Fe6:bicine and Fe6:tea cluster.

5 Conclusion

The study of the magnetic and electronic properties of the cyclic spincluster Fe6:bicine shows how the magnetic on-site anisotropy and the interaction between the Fe^{III} ions is influenced by a tiny modification of the coordinating and bridging ligand. The results confirm the magneto-structural correlation known for the tea ligand. High-frequency ESR provides insight into the structure of the excited spin states and reveals not only the importance of the fourth- and sixth-order spin operators in the description of the zero-field splitting but also the subtle effects of level crossings and mixing of spin states.

The authors thank Prof. E. Dormann for helpful discussions and the DFG for financial support under project PI336/2-1,2.

References

1. D. Gatteschi, A. Caneschi, L. Pardi, R. Sessoli, Science **265**, 1055 (1994); D. Gatteschi, A. Caneschi, R. Sessoli, A. Cornia, Chem. Soc. Rev. **25**, 101 (1996); A. Müller, F. Peters, M.T. Pope, and D. Gatteschi **98**, 239 (1998); P.C.E. Stamp, Nature (London) **383**, 125 (1996), B. Schwarzschild, Phys. Today **50**, 17 (1997)
2. A. Caneschi, A. Cornia, S.J. Lippard, Angew. Chem. **107**, 511 (1995); C. Benelli, S. Parsons, G.A. Solan, R.E.P. Winpenny, Angew. Chem. **108**, 1967 (1996); R.W. Saalfrank, I. Bernt, E. Uller, F. Hampel, Angew. Chem. **109**, 2596 (1997); S.P. Watton, R. Fuhrmann, L.E. Pence, A. Caneschi, A. Cornia, G.L. Abbati, S.J. Lippard, Angew. Chem. **109**, 2917 (1997)

3. A. Caneschi, A. Cornia, A.C. Fabretti, S. Foner, D. Gatteschi, R. Grandi, L. Schenetti, Chem. Eur. **2**, 1379 (1996); O. Waldmann, J. Schülein, R. Koch, P. Müller, I. Bernt, R.W. Saalfrank, H.P. Andres, H.U. Güdel, P. Allenspach, Inorg. Chem. **38**, 5879 (1999)
4. A. Cornia, A.G.M. Jansen, M. Affronte, Phys. Rev. B **60**, 12177 (1999); O. Waldmann, R. Koch, S. Schromm, J. Schülein, P. Müller, I. Bernt, R.W. Saalfrank, F. Hampel, E.Balthes, Inorg. Chem. **40**, 2986 (2001); Y. Shapira, V. Bindilatti, J. Appl. Phys. **92**, 4155 (2002)
5. A.-L. Barra, D. Gatteschi, R. Sessoli, Phys. Rev. B. **56**, 8192 (1997); A.-L. Barra, L.-C. Brunel, D. Gatteschi, L. Pardi, R. Sessoli, Acc. Chem. Res. **31**, 460 (1998)
6. B. Pilawa, R. Desquiotz, M.T. Kelemen, M. Weickenmeier, A. Geisselmann: J. Magn. Magn. Mater. **177-181**, 748 (1997); B. Pilawa, I. Keilhauer, R. Bofinger, D. Marinov, S. Knorr, A. Grupp, Appl. Magn. Reson. **21**, 527 (2001)
7. A. Geisselmann, Thesis Dissertation, Universität Karlsruhe (1998)
8. A. Geisselmann, Diploma-work Dissertation, Universität Karlsruhe (1996)
9. O. Waldmann, Europhys. Lett. **60**, 302 (2002)
10. G.F. Koster, J.O. Dimmock, R.G. Wheeler, H. Satz, (M.I.T. Pr., Cambridge, Mass. 1969)
11. L.D. Landau, E.M. Lifschitz, *Quantum mechanics* (Oxford, Butterworth-Heinemann, 1998); D. Gatteschi, L. Pardi, Gazzetta Chimica Italiana **123**, 1 (1993); O. Waldmann, Phys. Rev. B **61**, 6138 (2000)
12. The exact diagonalization of $\mathcal{H} = \mathcal{H}_{\rm ex} + \mathcal{H}_{\rm ligand} + \mathcal{H}_{\rm dipol} + \mathcal{H}_{\rm Zee}$ includes the energetically lowest eigenstates $S = 0$ (2 states), $S = 1$ (6 states), $S = 2$ (5 states), $S = 3$ (5 states) and $S = 4$ (1 state)
13. Two modifications of the Fe6:bicine system ($[Fe_6(bicine)_6]\cdot$2MeOH [7] and $[Fe_6(bicine)_6]\cdot$2EtOH [8]) were also prepared and investigated
14. The phenomenological description of the low temperature susceptibility becomes possible with an effective defect spin $S = 21/2$ and $D/k_B = 1.5$ K
15. I. Keilhauer, Thesis Dissertation, Universität Karlsruhe (to be published)